# CVS filtering and computation of turbulent mixing layers using orthogonal wavelets

**Kai Schneider**[1,2] **and Marie Farge**[3]

[1] **ICT, Universität Karlsruhe (TH) Kaiserstr. 12, 76128 Karlsruhe, Germany**
[2] **CMI, Université de Provence, 39 rue F. Joliot–Curie, 13453 Marseille Cedex 13, France**
[3] **LMD-CNRS, Ecole Normale Supérieure, 24 rue Lhomond, 75231 Paris Cedex 05, France**

## Abstract

We have introduced a new method [4], called CVS (Coherent Vortex Simulation), to compress and compute turbulent flows. It is based on the wavelet filtered Navier-Stokes equations and their solution in an adaptive wavelet basis [10]. Here we present applications[1] of the CVS method for two and three-dimensional turbulent mixing layers.

## 1 Introduction

In the turbulent regime the solutions of Navier–Stokes equations exhibit coherent vortices whose nonlinear interactions trigger the flow evolution. Since these coherent vortices are well localized and excited on a wide range of scales, we have proposed to use the wavelet representation of the vorticity field to extract them [4]. Orthogonal wavelet bases are well suited for this, because they are made of self-similar functions localized in both physical and spectral spaces [3], [1]. In [4] we have introduced a new method, called CVS (Coherent Vortex Simulation), to compute turbulent flows. It is based on the wavelet filtered Navier-Stokes equations and their solution in an adaptive wavelet basis [10]. Here we present applications of the CVS method to 2D and 3D turbulent flows. The paper is organized in two parts: coherent vortex extraction and CVS computation. We first present the wavelet algorithm to extract coherent vortices and we apply it to a 3D turbulent mixing layer. We then compare these results with those obtained , for the same compression, using a low-pass filter, as it is done witth LES computation. In the second part we sketch the adaptive wavelet Navier-Stokes solver which is used for the CVS computation. We apply it to calculate a 2D temporally growing mixing layer and compare the results thus obtained with those of a classical DNS computed using a pseudo-spectral method.

## 2 Coherent vortex extraction of a 3D mixing layer

### 2.1 Wavelet method for coherent vortex extraction

We have proposed [4], [6] a wavelet-based method to extract coherent vortices out of 2D and 3D turbulent flows. In the following we will describe the algorithm for the 3D case computed at resolution $N = 2^J$, $J$ being the number of octaves. We consider the vorticity field $\vec{\omega}(\vec{x}) = \nabla \times \vec{V}$ and develop each component as an orthogonal wavelet series from the largest scale $l_{max} = 2^0$ to the smallest scale $l_{min} = 2^{J-1}$ using a 3D multi-resolution analysis (MRA) [1], [3]:

$$\omega(\vec{x}) = \bar{\omega}_{0,0,0}\ \phi_{0,0,0}(\vec{x}) + \sum_{j=0}^{J-1} \sum_{i_x=0}^{2^j-1} \sum_{i_y=0}^{2^j-1} \sum_{i_z=0}^{2^j-1} \sum_{\mu=1}^{2^n-1} \tilde{\omega}^{\mu}_{j,i_x,i_y,i_z}\ \psi^{\mu}_{j,i_x,i_y,i_z}(\vec{x}),$$

with $\phi_{j,i_x,i_y i,i_z}(\vec{x}) = \phi_{j,i_x}(x)\ \phi_{j,i_y}(y)\ \phi_{j,i_z}(z)$, and

$$\psi^{\mu}_{j,i_x,i_y,i_z}(\vec{x}) = \begin{cases} \psi_{j,i_x}(x)\ \phi_{j,i_y}(y)\ \phi_{j,i_z}(z)\ ; & \mu = 1, \\ \phi_{j,i_x}(x)\ \psi_{j,i_y}(y)\ \phi_{j,i_z}(z)\ ; & \mu = 2, \\ \phi_{j,i_x}(x)\ \phi_{j,i_y}(y)\ \psi_{j,i_z}(z)\ ; & \mu = 3, \\ \psi_{j,i_x}(x)\ \psi_{j,i_y}(y)\ \psi_{j,i_z}(z)\ ; & \mu = 4, \\ \psi_{j,i_x}(x)\ \psi_{j,i_y}(y)\ \phi_{j,i_z}(z)\ ; & \mu = 5, \\ \phi_{j,i_x}(x)\ \psi_{j,i_y}(y)\ \psi_{j,i_z}(z)\ ; & \mu = 6, \\ \psi_{j,i_x}(x)\ \psi_{j,i_y}(y)\ \psi_{j,i_z}(z)\ ; & \mu = 7, \end{cases}$$

where $\phi_{j,i}$ and $\psi_{j,i}$ are the one-dimensional scaling function and the corresponding wavelet, respectively. Due to the orthogonality, the scaling coefficients are given by $\bar{\omega}_{0,0,0} = \langle \omega\ ,\ \phi_{0,0,0} \rangle$ and the wavelet coefficients are given by $\tilde{\omega}^{\mu}_{j,i_x,i_y,i_z} = \langle \omega\ ,\ \psi^{\mu}_{j,i_x,i_y,i_z} \rangle$, where $\langle \cdot, \cdot \rangle$ denotes the $L^2$-inner product.

We then apply the threshold $\epsilon = (4/3Z \log N)^{1/2}$, where $Z$ is the total enstrophy and $N$ the resolution, to the wavelet coefficients of vorticity. The advantage of our method is that the threshold is objective and therefore has no adjustable parameters. The choice of the threshold is based on theorems derived by Johnstone and Donoho [2], which have proved the optimality of the wavelet representation to denoise signals in presence of Gaussian white noise. The coherent vorticity field $\vec{\omega}_C$ is reconstructed from the wavelet coefficients whose modulus is larger than $\epsilon$ and the incoherent vorticity field $\vec{\omega}_I$ from the wavelet coefficients whose modulus is smaller or equal to $\epsilon$. The two fields thus obtained, $\vec{\omega}_C$ and $\vec{\omega}_I$, are orthogonal, which ensures a separation of the total enstrophy into $Z = Z_C + Z_I$ because the interaction term $\langle \vec{\omega}_C\ , \vec{\omega}_I \rangle$ is zero. We then use Biot–Savart's relation $\vec{V} = \nabla \times (\nabla^{-2} \psi)$ to reconstruct the coherent velocity $\vec{V}_C$ and the incoherent velocity $\vec{V}_I$.

### 2.2 Numerical results

In the present paper we apply the above algorithm to a high resolution DNS ($N = 512 \times 256 \times 128$) of a forced turbulent mixing layer [7] to check the potential for the CVS method to extract coherent vortices in 3D shear flows. Fig. 1 show the modulus of vorticity for the total flow. We observe many longitudinal vortex tubes resulting from a 3D instability, called ribs, which are wrapped

[1]The paper has been written during the CEMRACS 2000 workshop at CIRM, Université d'Aix–Marseille. We gratefully acknowledge financial support and hospitality.

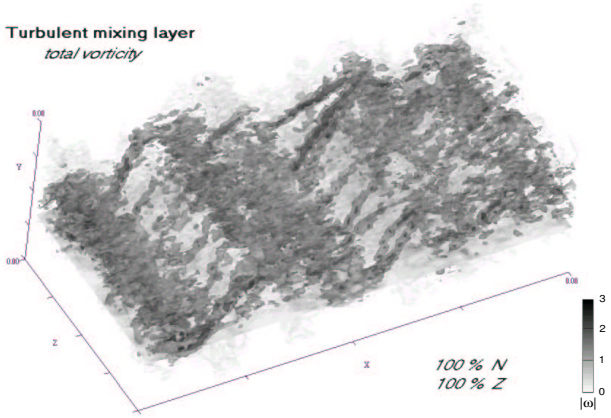


Figure 1: Total vorticity of the 3D turbulent mixing layer at low resolution $N = 64^3$.

onto four transversal rollers, produced by a 2D Kelvin–Helmholtz instability.

The coherent part (see Fig. 2 top), which represents $5.7\%$ (at low resolution $N = 64^3$) or $3\%$ (at high resolution $N = 512 \times 256 \times 128$) of the total number of coefficients, captures most of the turbulent kinetic energy and enstrophy, even at high wavenumbers. Moreover, the pdf of coherent vorticity is similar to that of the total flow (see Fig. 3). The incoherent part (see Fig. 2 bottom), which represents $97\%$ (at low resolution $N = 64^3$) or $94.3\%$ (at high resolution $N = 512 \times 256 \times 128$) of the total number of coefficients, contains little of the turbulent kinetic energy and enstrophy. It is nearly homogenenous with a very low amplitude and contains no structure.

The corresponding 1D energy spectra in the streamwise direction shows that the coherent part presents, all along the inertial range, the same correlation as the total flow, while the incoherent part contains very little energy and is well decorrelated.

### 2.3 Comparison between CVS and LES filtering

In Fig. 3 we compare the CVS and the LES filterings for the same number of retained coefficients ($3\%N$). Since the LES filtering retains only the low wavenumbers (Fig. 3 top, right), the coherent vortices are smoothed and as a result the variability of the vorticity field is strongly reduced (see PDF on Fig. 3 bottom, right). In contrast, the CVS filtering retains the organized vortices, whatever their scales are, and as a results the shape of the vorticity PDF is preserved, even for large values of $|\omega|$ (Fig. 3 bottom, left).

Concerning turbulence parametrization, i.e. the statistical modelling of the effect of the discarded modes onto the retained modes, we can draw the following conclusion:

- The CVS filtering allows to disentangle the organized and random components of turbulent flows. As a results the discarded incoherent modes have very weak amplitude, are almost homogeneous in space and are well decorrelated, which controls the risk of backscattering, i.e. the transfers from the discarded modes into the resolved modes.

- The LES filtering does not decorrelate the high-wavenumber modes and, as a result, there are many organized structures present in those modes. Moreover, the variability of the total field is not retained by the LES filtering and, as a consequence, the discarded high-wavenumber modes present much higher amplitude of the vorticity than the incoherent modes discarded by the CVS filtering. Those two drawbacks of the LES filtering lead to the development of nonlinear instabilities, which may trigger backscatter.

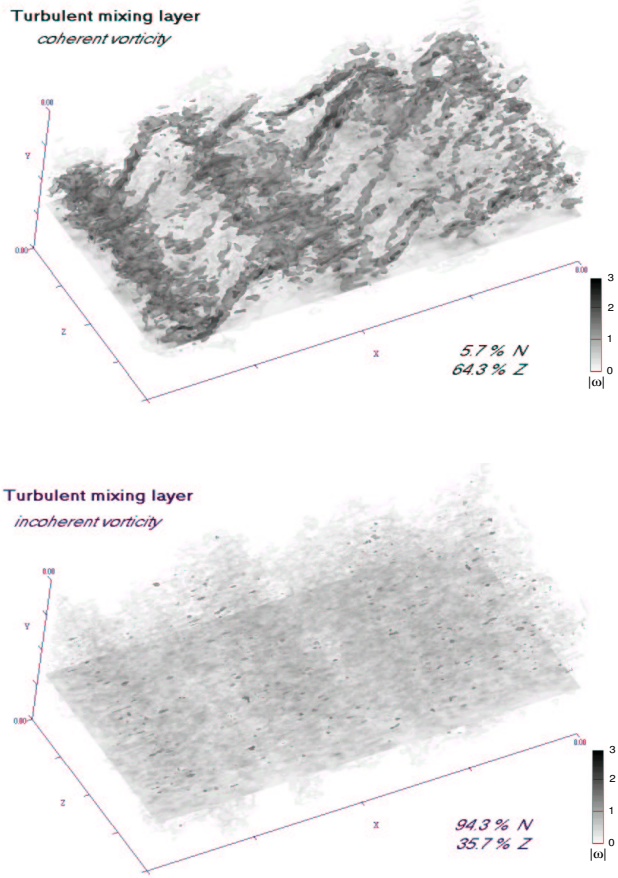


Figure 2: Top: Coherent vorticity of the 3D turbulent mixing layer at low resolution $N = 64^3$, reconstructed from $5.7\%$ of the wavelet coefficients and containing $64.3\%$ of the total enstrophy. Bottom: Incoherent vorticity reconstructed from $94.3\%$ of the wavelet coefficients and containing $35.7\%$ of the total enstrophy.

We conjecture that the derivation of a turbulence model is easier with a CVS filtering than with a LES filtering. However, the CVS filtering requires a dynamically adaptive mesh refinement for solving Navier–Stokes equations. In the next section we present such a method based on the wavelet representation that we have developed for the 2D Navier–Stokes equations.

## 3 CVS computation of a 2D mixing layer

### 3.1 Adaptive wavelet method for 2D Navier–Stokes equations

In the following we briefly sketch the adaptive wavelet method. For further details we refer to [9, 10]. We consider the Navier–Stokes equations written in velocity-vorticity formulation

$$\partial_t \omega + \mathbf{v} \cdot \nabla \omega = \nu \nabla^2 \omega \,, \qquad \nabla \cdot \mathbf{v} = 0 \,, \tag{1}$$

with the velocity field $\mathbf{v} = (u, v)$, the vorticity $\omega = \nabla \times \mathbf{v}$ and the kinematic viscosity $\nu$. We assume periodic boundary conditions in both directions.

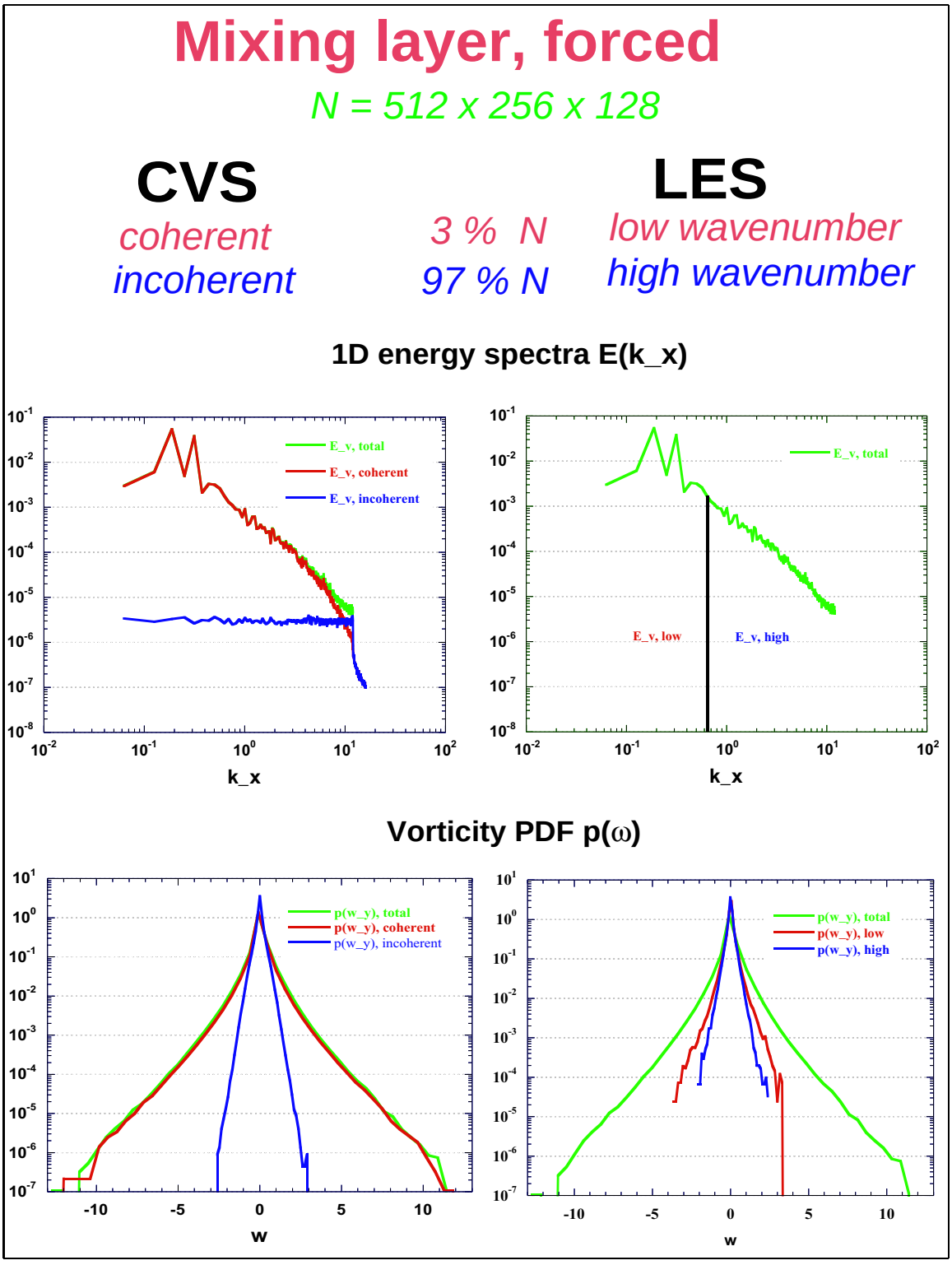


Figure 3: Comparison of CVS (left) with LES (right) filtering for the 3D mixing layer at resolution $N = 512 \times 256 \times 128$. Energy spectra (top) and PDF of vorticity (bottom) of total, coherent and incoherent flow using CVS filtering and of low wavenumber and high wavenumber components using LES filtering.

For the time discretization we use finite differences with a semi-implicit scheme, i.e. backward–differences for the viscous term and Adams–Bashforth extrapolation for the nonlinear term, both of second order. We obtain

$$(\gamma I - \nu\nabla^2)\omega^{n+1} = \frac{4}{3}\gamma\omega^n - \frac{1}{3}\gamma\omega^{n-1} - \mathbf{v}^\star \cdot \nabla\omega^\star, \quad (2)$$

where $\omega^\star = 2\omega^n - \omega^{n-1}$, with time step $\Delta t$, $\gamma = 3/(2\Delta t)$ and $I$ representing the identity.

For the spatial discretization we use a Petrov–Galerkin scheme. Therefore the vorticity is expanded into a set of trial functions and the minimization of the weighted residual of (2) requires that the projection onto a space of test functions vanishes.

As space of trial functions we employ a 2D multires-

olution analysis, and expand $\omega^n$ at time step $n$ into an orthonormal wavelet series, from the largest scale $l_{max} = 2^0$ to the smallest scale $l_{min} = 2^{-J+1}$:

$$\omega^n(x,y) = \sum_{j=0}^{J-1} \sum_{k_x,k_y=0}^{2^j-1} \sum_{d=1}^{3} \tilde{\omega}_\lambda^n \psi_\lambda(x,y) \,, \qquad (3)$$

where $\lambda = (j, k_x, k_y, d)$ . One consequence of the orthogonality of the trial functions is that we know exactly what amount of enstrophy is lost in the remeshing step.

The test functions $\theta_\mu$ used here are defined as solutions of the linear part of equation (2), i.e.

$$(\gamma I - \nu\nabla^2)\theta_\mu = \psi_\mu \,. \qquad (4)$$

Hence,

$$\langle (\gamma I - \nu\nabla^2)\psi_\lambda \,,\, \theta_\mu \rangle = \langle \psi_\lambda \,,\, (\gamma I - \nu\nabla^2)\theta_\mu \rangle = \delta(\lambda - \mu) \,.$$

This avoids the assembly of the stiffness matrix and the solution of a linear equation at each time step. The functions $\theta_\mu$, called vaguelettes, are explicitly calculated in Fourier space and have localization properties similar to wavelets.

The solution of (2) therewith reduces to a simple change of basis,

$$\begin{aligned} \omega_\lambda^{n+1} &= \langle \omega^{n+1} \,,\, \psi_\lambda \rangle \\ &= \langle \frac{4}{3}\gamma\omega^n - \frac{1}{3}\gamma\omega^{n-1} - \mathbf{v}^\star \cdot \nabla\omega^\star \,,\, \theta_\lambda \rangle \,. \end{aligned} \qquad (5)$$

An adaptive discretization is obtained by applying at each time step a nonlinear wavelet thresholding technique which retains only wavelet coefficients $\tilde{\omega}_\lambda^n$ with absolute value above a given threshold $\epsilon = \epsilon_0\sqrt{Z}$, where $Z = \frac{1}{2}\int \omega^2 dx$. For the next time step the index coefficient set (which addresses each coefficient in wavelet space) is determined by adding neighbours to the retained wavelet coefficients, consequently only those coefficients $\omega_\lambda$ in (5), belonging to this extrapolated index set, are computed using the adaptive vaguelette decomposition. The vorticity $\omega^\star$ is reconstructed in physical space on an adaptive grid from its wavelet coefficients $\{\tilde{\omega}_\lambda^\star\}$ using the adaptive wavelet reconstruction algorithm. The nonlinear term $\mathbf{v}^\star \cdot \nabla\omega^\star$ is evaluated by partial collocation on a locally refined grid.

Using the adaptive vaguelette decomposition with $\theta = (\nabla^2)^{-1}\psi$, we solve $\nabla^2\Psi^\star = \omega^\star$ ($\Psi^\star$ being the stream function), get $\{\Psi_\lambda^\star\}$ and finally reconstruct $\Psi^\star$ on the refined grid. By means of centered finite differences of 4th order we finally compute $\nabla\omega^\star$ and $\mathbf{v}^\star = (-\partial_y\Psi^\star, \partial_x\Psi^\star)$ on the adaptive grid and we evaluate the nonlinear term pointwise. Subsequently (5) can be solved using the adaptive vaguelette decomposition. A complete description of this algorithm is given in [9, 10]. Finally, let us mention that the total complexity of the algorithm is of order $O(N_{ad})$, where $N_{ad}$ denotes the number of wavelet coefficients retained in the adapted basis. As the present implementation has not yet been optimized, the computing time is as effective as a classical spectral method for the resolution used here ($N = 256^2$).

### 3.2 Numerical results

In [10, 4] we studied a temporally developing mixing layer, schematically sketched in Fig. 4. The initial velocity has a hyperbolic–tangent profile $u(y) = U\tanh(2y/\delta_0)$ which implies a vorticity thickness $\delta_0 = 2U/(du/dy)|_{y=0}$. From linear stability analysis the mixing layer is known to be inviscidly unstable. A perturbation leads to the formation of vortices by Kelvin–Helmholtz instability, where the most amplified mode corresponds to a longitudinal wavelength $\lambda = 7\delta_0$.

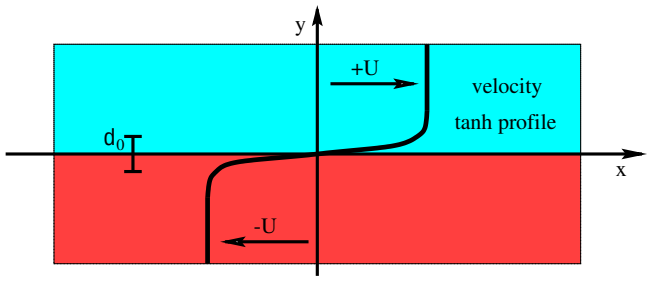


Figure 4: Initial configuration for the mixing layer.

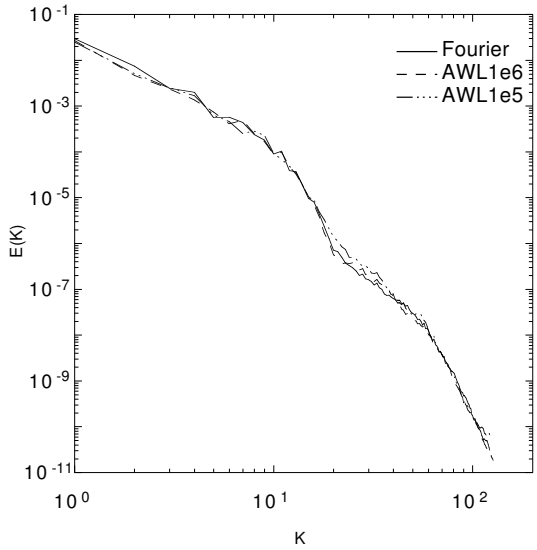


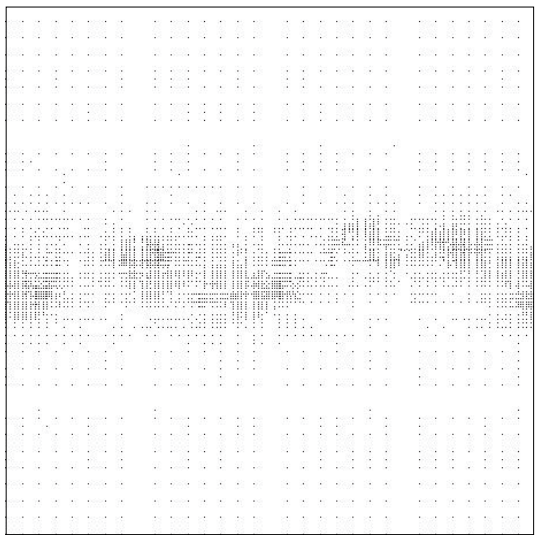

Figure 5: Top: energy spectra for the pseudo–spectral reference run and for the adaptive wavelet simulations with thresholds $\epsilon_0 = 10^{-6}, 10^{-5}$. Bottom: adaptive grid reconstructed from the index set of the retained wavelet coefficients. Both at time $t = 37.5$.

The initial vorticity thickness $\delta_0$ is chosen such that 10 vortices should develop in the numerical domain of size $[0, 2\pi]^2$. To trigger the instability we superimposed

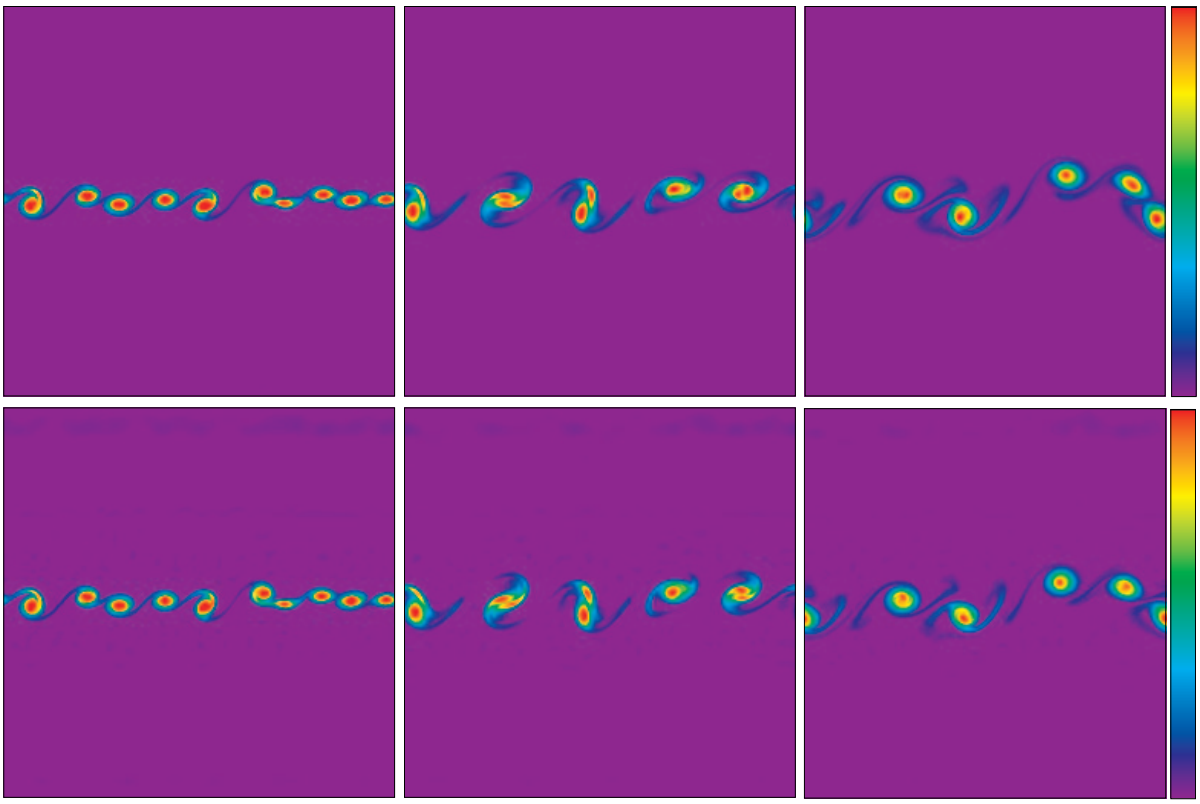

Figure 6: $\omega$ at $t = 12.5,\ 25,\ 37.5$. Top: pseudo–spectral method (vorticity-based). Bottom: adaptive wavelet method ($\epsilon_0 = 10^{-6}$).

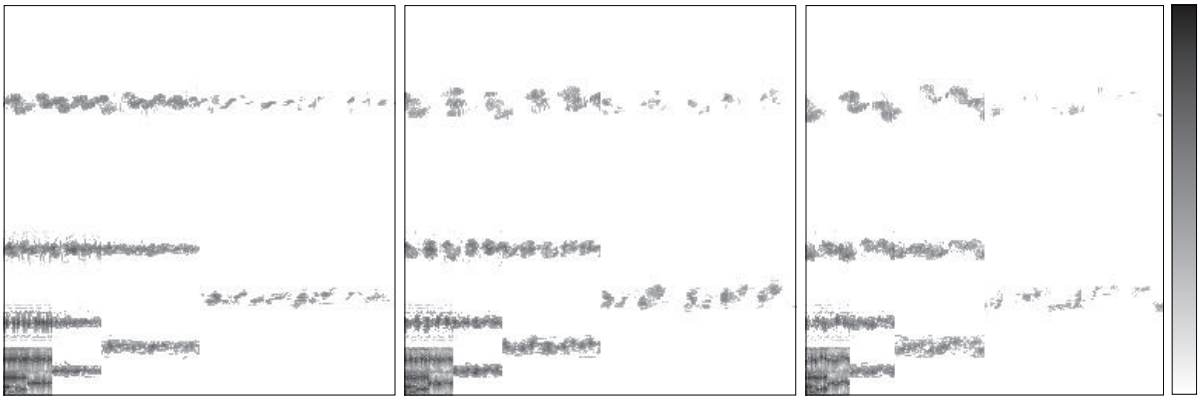

Figure 7: Active wavelet coefficients at $t = 12.5,\ 25,\ 37.5$. ($\epsilon_0 = 10^{-6}$).

a weak white noise in the rotational region. The velocity is $U \approx 0.1035$ and the viscosity is $\nu = 5 \cdot 10^{-5}$.

For the numerical simulation we employ a maximal resolution of $N = 256^2$, which corresponds to $J = 8$ in (3), and cubic spline wavelets of Battle–Lemarié type. The time step is $\Delta t = 2.5 \cdot 10^{-3}$. The threshold for the wavelet coefficients is $\epsilon_0 = 10^{-6}$ or $10^{-5}$.

In Fig. 5 (top) we compare the energy spectrum at $t = 37.5$ for a reference computation using a classical pseudo-spectral method at resolution $n = 256^2$, and for two wavelet computations using different thresholds ($\epsilon_0 = 10^{-6}$ and $10^{-5}$).

Fig. 5 (top) shows that all scales of the flow are well-resolved for both thresholds. The underlying grid Fig. 5 (bottom) which corresponds to the centers of active wavelets for the computation with $\epsilon_0 = 10^{-6}$ at $t = 37.5$ shows a local refinement in regions of strong gradients where dissipation is most active.

### 3.3 Comparison between CVS and Fourier pseudo-spectral DNS

In Fig. 6 (bottom) we show the evolution of the vorticity field for the adaptive wavelet simulation with threshold $\epsilon_0 = 10^{-6}$ and for the reference pseudo–spectral computation (top). In both simulations, as predicted by the linear theory, 10 vortices are formed, which subsequently undergo successive mergings. In Fig. 7 the active wavelet coefficients (gray entries) are plotted using a logarithmic scale. The coefficients $\tilde{\omega}_\lambda$ are placed at position $(x_1, x_2) = (2^j(1-\delta_{d,1})+k_x, 2^j(1-\delta_{d,2})+k_y$, $\delta$ being the Kronecker tensor, with the origin in the lower left corner and the $y$-coordinate oriented upwards, from coarser to finer scales. We observe that the basis dynamically adapts to the flow evolution during the computation with only $8\%$ of the coefficients being used. In the wavelet simulation the formation and evolution of vortices are as well captured as in the reference run (top). This might be due to

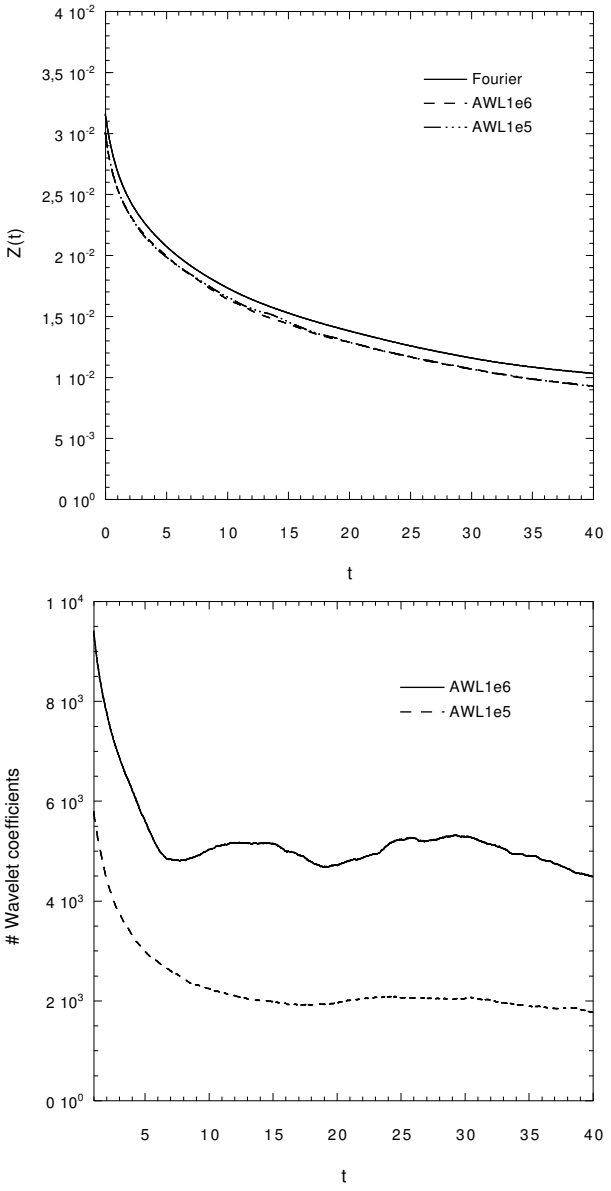


Figure 8: Comparison between DNS and CVS with $\epsilon_0 = 10^{-6}$ and $10^{-5}$. Top: evolution of enstrophy. Bottom: evolution of the number of degrees of freedom for $\epsilon_0 = 10^{-6}$ and $10^{-5}$.

the fact that the retained wavelet coefficients contain 94% of the total enstrophy, as observed in Fig. 8 (top) which shows the time evolution of the total enstrophy using the different thresholds.

We observe a 6% loss of enstrophy which comes from the fact that in the wavelet simulations we have not modelled the effect of the discarded modes onto the retained ones, similarly to the subgrid scale model used in LES. This will be considered in future work, where the enstrophy of the discarded wavelets will be reinjected into the coherent vortices using the wavelet forcing method we have proposed [8].

Finally, we plot the time evolution of the number of degrees of freedom for the two wavelet runs in Fig. 8 (bottom). First, we observe an initial phase, up to $t = 7$ s, where there is a strong reduction in the number of active modes, which corresponds to the formation of the coherent vortices. Then, the number of active modes remains almost constant, which represent a significant reduction of the number of modes, with $N_{ad} = 5000$ for $\epsilon_0 = 10^{-6}$ and $N_{ad} = 2000$ for $\epsilon_0 = 10^{-5}$, out of $N = 256^2 = 65536$ initail modes.

## 4 Conclusion

We have proposed the CVS method to compress and compute turbulent flows. It is based on the projection of the vorticity field onto an orthogonal wavelet basis and the decomposition of the vorticity field into two orthogonal components, using a nonlinear thresholding of the wavelet coefficients. The coherent vorticity field is reconstructed from the few wavelet coefficients larger than a given threshold, which depends only on the resolution and on the total enstrophy, while the incoherent vorticity is reconstructed from the many remaining weak wavelet coefficients. The coherent and incoherent velocity fields are then derived from the coherent and incoherent vorticity fields using Biot–Savart's equation.

In this paper we have applied this method to a 3D mixing layer computed at resolution $N = 512 \times 256 \times 128$. We have shown that the coherent flow corresponds to only $3\%N$ wavelet modes, presents the same non-Gaussian PDF of vorticity and retains most of the energy and enstrophy, with the same spectral distribution, as the total flow. Moreover, the remaining incoherent flow is structureless, exhibits a much narrower PDF of vorticity with an exponential distribution and presents an energy equipartition spectrum. This ensures the possibility to parametrize the effect of the incoherent flow onto the coherent flow with a low-order statistical model. For LES the subgrid scale modelling is much more difficult to parametrize, since we have shown that the small scale flow, which is discarded in LES, exhibits many coherent structures, has a much wider PDF of vorticity and does not present an energy equipartition spectrum.

We have then presented an adaptive wavelet computation of a 2D mixing layer and shown the dynamical adaption of the grid in physical space, which allows to follow the flow evolution with a reduced number of active degrees of freedom. The CVS computation combines an Eulerian representation of the flow with a Lagrangian adaption strategy of the active degrees of freedom to be computed. We will now extend this method to 3D Navier–Stokes equations, since we have shown in this paper that the compression obtained with the CVS filtering applied to a 3D mixing layer is important and that the CVS computation of a 2D mixing layer gives the same results as those from a standard DNS.

## Acknowledgements:

We thank Giulio Pellegrino for the 3D wavelet code and Mike Rogers for providing us the 3D fields from his turbulent mixing layer computation. The CVS filtering of the 3D turbulent mixing layers has been done during the CTR Summer programme 2000 at NASA Ames/Stanford University and we thankfully acknowledge financial support from CTR.

## Bibliography

[1] I. Daubechies. *Ten Lectures on wavelets*. SIAM, Philadelphia, 1992.

[2] D. Donoho. Unconditional bases are optimal bases for data compression and statistical estimation, *Appl. Comput. Harmon. Anal.* **1** (1993), 100.

[3] M. Farge. Wavelet Transforms and their Applications to Turbulence. *Ann. Rev. of Fluid Mech.*, **24**, 395–457, 1992.

[4] M. Farge, K. Schneider and N. Kevlahan. Non–Gaussianity and Coherent Vortex Simulation for two–dimensional turbulence using an adaptive orthonormal wavelet basis. *Phys. Fluids*, **11**(8), 2187–2201, 1999.

[5] M. Farge and K. Schneider. Coherent Vortex Simulation (CVS), a semi-deterministic turbulence model using wavelets. *Flow, Turb. Combust.*, submitted.

[6] M. Farge, G. Pellegrino and K. Schneider. Coherent vortex extraction in 3D turbulent flows using orthogonal wavelets. Preprint, 2000, submitted to *Phys. Rev. Lett.*.

[7] M. Rogers and R. Moser. Direct simulation of a self-similar turbulent mixing layer. *Phys. Fluids*, **6**(2), 903–923, 1994.

[8] K. Schneider and M. Farge. Wavelet forcing for numerical simulation of two-dimensional turbulence, *C. R. Acad. Sci. Paris, série II b*, **325**, 263–270, 1997.

[9] K. Schneider and M. Farge. Wavelet approach for modelling and computing turbulence. *Lecture Series 1998–05 Advances in turbulence modelling*, von Karman Institute for Fluid Dynamics, Bruxelles, 132 pages, 1998.

[10] K. Schneider and M. Farge. Numerical simulation of temporally growing mixing layer in an adaptive wavelet basis. *C. R. Acad. Sci. Paris Série II b*, **328**, 263–269, 2000.